EUROPEAN COMMISSION

HORIZON 2020 PROGRAMME
TOPIC H2020-LCE-07-2016-2017
Developing the next generation technologies of renewable electricity and heating/cooling

GA No. 727523

Next – generation interdigitated back-contacted silicon heterojunction solar cells and modules by design and process innovations

NEXTBASE
THE NEXT GENERATION BASELINE

NextBase - Deliverable report

D8.5 – Report on a pathway to reach the efficiencies defined in the project goals, and beyond.

Deliverable No.	NextBase D8.5	
Related WP	WP8	
Deliverable Title	Report on a pathway to reach the efficiencies defined in the project goals, and beyond.	
Deliverable Date		
Deliverable Type	Report	
Dissemination level	Public (PU)	
Author(s)	Paul Procel (TUD), Olindo Isabella (TUD), Miro Zeman (TUD)	02-2019
Checked by	Bertrand Paviet-Salomon, Olindo Isabella (TUD), Antonin Fejfar (FZU)	03-2019
Reviewed by (if applicable)	WP leaders	03-2019
Approved by	Kaining Ding (Jülich) - Coordinator	27-03-2019
Status	Final	

Disclaimer/ Acknowledgment

This project has received funding from the European Union's Horizon 2020 research and innovation programme under grant agreement No 727523. The information and views set out in this publication does not necessarily reflect the official opinion of the European Commission. Neither the European Union institutions and bodies nor any person acting on their behalf, may be held responsible for the use which may be made of the information contained therein.

Publishable summary

The path for achieving high efficiency (IBC-) SHJ solar cells is established in terms of layers properties, using contact resistivity ρ_c and rear side patterning as figures of merit for optimal charge carriers transport. Practical insights are provided on how to improve the transport and collection of carriers in terms of activation energy and carrier concentration of transparent conductive oxide (TCO) and their relation in the estimation of contact resistivity. Furthermore, as minimal contact resistivity values are associated additionally to low recombination in thin silicon films, evaluating contact resistivity is a practical indicator for contact stack quality.

In general, contact resistivity is minimal (maximal conversion efficiency) using doped layers exhibiting low activation energy values, which are experimentally achievable in thin-film nano-crystalline Si layers. Using those, the device is resilient against work-function mismatch or TCO material choice (e.g. AZO, IOH or ITO). N-contact stack using doped nano-crystalline layers or TCO with high carrier concentration facilitates contact resistivity values below 40 $m\Omega \cdot cm^2$ with potential fill factor (FF) higher than 85% meaning conversion efficiency higher than 26%. P-contact stack using doped nano-crystalline layers together with TCO featuring high carrier concentration facilitates, again, contact resistivity values lower than 50 $m\Omega \cdot cm^2$ with potential FF above 85% and consequently efficiency values higher than 26%.

Finally, lateral transport inside the bulk is evaluated in terms of pitch and width of n-type and p-type contacts. Small pitch values increase FF. Specifically for IBC-SHJ cells, n-type and p-type contacts should cover the pitch according to contact resistivity of n- and p-contact ratio. A minimal half-pitch value of 800 µm to attain FF above 85% is identified. Such a patterning is feasible for processes that commonly include costly photo-lithography technology. However, industry attractive single patterning using shadow mask (tunneling IBC - half pitch values > 1000 µm) also potentially could achieve efficiency above 26 % with fine tuning of half pitch and reducing bulk thickness to 200 µm.

Contents

List of acronyms, abbreviations and definitions

Table 1.1 Acronym table

Abbreviation	Explanation
AZO	Aluminium-doped zinc oxide
B2BT	Band to band tunnelling
c-Si	Crystalline silicon
DT	Direct tunnelling
E_a	Activation energy
FF	Fill Factor
***i-a*-Si:H**	Intrinsic hydrogenated amorphous silicon
IBC	Interdigitated back contact
ITO	Indium tin oxide
J_{sc}	Shor-circuit current density
N_{TCO}	Transparent conductive oxide carrier concentration
SRH	Shockley–Read–Hall recombination
TAT	Trap assisted tunnelling
TCAD	Technology computer aided design
TCO	Transparent conductive oxide
TLM	Transmission line measurement
V_{oc}	Open-circuit voltage
η	Solar cell conversion efficiency
ρ_c	Contact resistivity

1 Introduction

SHJ concepts are based on thin-film Si alloys, TCO and metallization as a contact system that enables efficient carrier collection while repelling non-collecting carriers. Interestingly, thin-film Si technology allows flexibility to develop layers in a wide range of fabrication parameters (J. McCann, R. Catchpole, J. Weber, & W. Blakers, 2001; Lee & Ebong, 2017; Yamamoto et al., 2015) thanks to the remarkable experience in PV field. Indeed, there is a broad list of thin-film based on alloys of Si with carbon, oxygen or nitrogen in different phases: amorphous and nano-crystalline. Similarly, TCOs films feature different opto-electrical properties depending on oxide base compound (i.e. ZnO usually Al-doped - AZO, In_2O_3 usually Sn-doped - ITO) (Klein et al., 2010). Typically, SHJ technology exhibits outstanding passivation in terms of V_{oc} while IBC architectures improve photons collections in terms of high J_{sc} values. Indeed, D3.3 reports the conditions for achieving $J_{sc} > 42$ mA/cm^2. In this document, FF and V_{oc} are investigated as FF is the core for achieving high efficiency SHJ solar cells (Adachi, Hernández, & Yamamoto, 2015; Yoshikawa et al., 2017). Physical mechanisms ruling FF are typically associated to resistive losses that are also linked to materials conductivity and contact resistivity (ρ_c). However, carrier transport phenomena can truly describe the inner physics of carrier collection as the core of FF (Procel, Yang, Isabella, & Zeman, 2018). In this context, the use of advanced simulation tools is essential to understand the competitive physical mechanisms that affect carrier's collection inside IBC-SHJ solar cells and their impact also on ρc.

Deliverable D8.5 is related to task 8.3, which aims at providing inputs to WPs 3-5 regarding materials and interface properties required to maximize conversion efficiency of IBC-SHJ solar cells. Accordingly, it summarises simulation efforts and related analysis of IBC-SHJ solar cells aiming at essential properties of layers in order to build contact stack for high performance devices (WP4) including the patterning design (WP5).

Deliverable Number	Deliverable name	Lead partner	Type	Dissemination level	Due date
D8.5	Report on a pathway to reach the efficiencies defined in the project goals, and beyond	TUD	R	PU	M30

2 Carrier collection mechanisms in SHJ solar cells

In IBC-SHJ solar cells, collection of carriers involves transport through two hetero-interfaces: c-Si / i-a-Si:H and doped layer / TCO. Such hetero-interfaces exhibit discontinuities in the band diagram, building so-called energy barriers (see dashed areas in Figure 1a and 1b). In either the n-type or p-type contact stack, the potential barrier for electron (hole) are illustrated as the area under (above) the curve of conduction (valence) band between the two abovementioned interfaces. Transport of carriers through these energy barriers is described by two mechanisms: i) thermionic emission and ii) tunnelling. Both models are associated to transport of carriers across energy barriers or discontinuities. Basic tunnelling implies three conditions: i) band alignment, ii) energy barrier size and iii) accumulation vs available electronic states at both sides of the potential barrier (Gehring & Selberherr, 2004). As Figure 1 shows, in SHJ structures, Si-based deposited film build the energy barrier while concurrently controlling the band bending in c-Si (ϕ) that rules the carrier accumulation of electrons for n-contact or holes for p-contact (Procel et al., 2018). In particular, energy barrier size tends to be more favourable for electrons than holes due to the asymmetric band offset resulting from the inherent electronic band structure of SHJ hetero-interfaces.

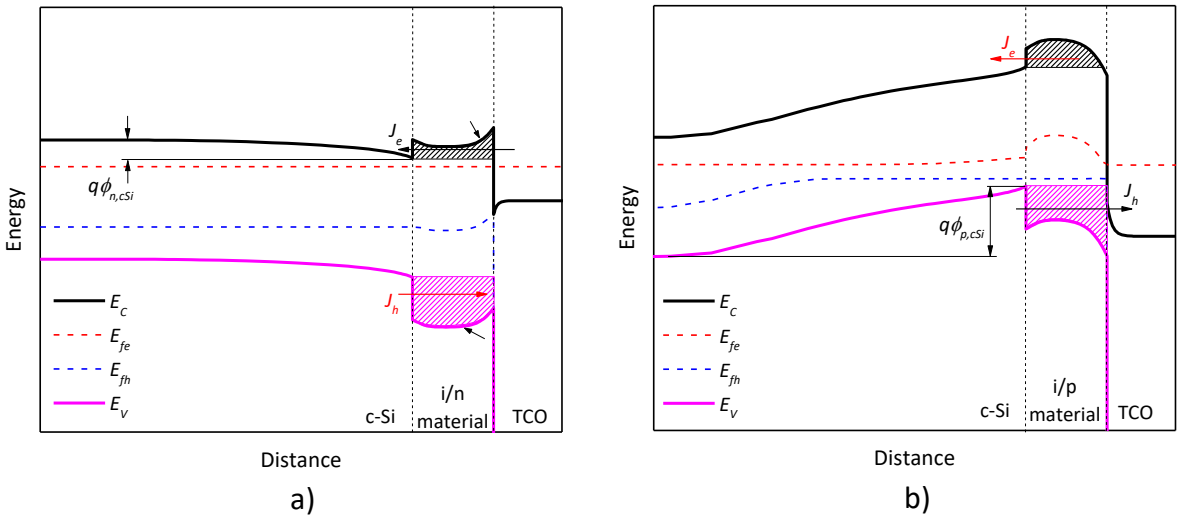

Figure 1. Schematic band diagram of n-type (a) and p-type (b) contacts of a SHJ solar cell under illumination. E_C (E_V) and E_{fe} (E_{fh}) are conduction (valence) band energy level and Quasi-Fermi level of electrons (holes); $q\phi_{n,cSi}$ ($q\phi_{p,cSi}$) is the band bending at the c-Si / i-a-Si:H interface for n-type contact (p-type contact). Patterned areas stand for energy barriers for electrons in conduction band and for holes in valence band. (Procel et al., 2018)

The band alignment occurs in the conduction band (c-Si, n-layer and TCO) in direct tunnelling (DT) mechanisms for n-contact. For p-contact, the band alignment happens from valence band (c-Si and p-layer) to the conduction band at TCO in the so-called band to band tunnelling (B2BT) in ideal conditions. For both contacts, the availability of states at TCO depends on the position of the conduction relative to electron quasi-Fermi energy. It is worth noting that thin-film Si materials are defective, exhibiting additional states due their disordered nature and dangling bonds (Powell &

Deane, 1996), thus supporting tunnelling mechanisms in sub-gap states or trap-assisted tunnelling (TAT). In SHJ, such a phenomenon is apparent in the p-contact, in absence of band alignment for collecting positive charge as Figure 2 b) and c) depicts. In case of n-contact (see Figure 2 a)), however, TAT is outnumbered by more efficient DT. Interestingly, aforementioned tunnelling mechanisms can be controlled by the relative position of conduction or valence band with respect to Fermi energy of deposited layers and TCO. In fact, for thin-film Si, the absolute value of the energy difference between conduction or valence band is quantified in terms of activation energy that is a practical measurable parameter. In case of TCO, the position of conduction band depends on the amount of dopants (Sn for ITO or Al for AZO) and shallow defects measured in terms of carrier concentration. In the following, we report the path for achieving high efficiency IBC-SHJ in terms of i) layers parameters and ii) rear side patterning.

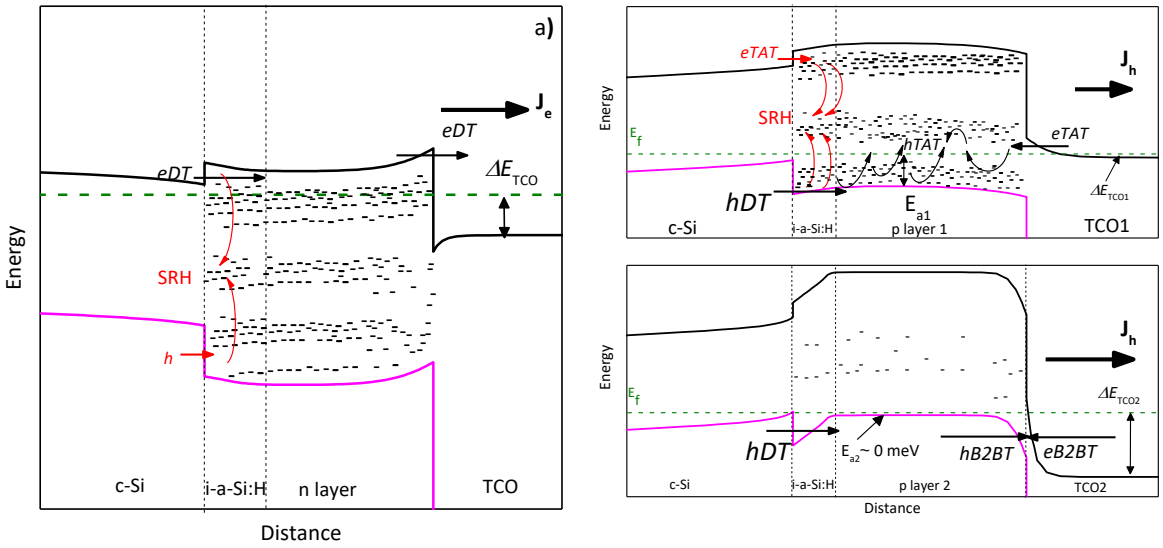

Figure 2. Equilibrium band diagram illustrating possible tunneling processes for (a) n-contact stack and (b and c) p-contact stack. a) Transport through n-contact is based on DT mechanisms; defects in deposited layers impact on SRH depending on selectivity of the contact. Transport through p-contact stack is based on b) TAT and c) B2BT. In b), the TCO conduction band (E_C) is not aligned with the valence band (E_V) at c-Si or p-layer. N_{TCO1} is not high enough to pull down the TCO E_C (ΔE_{TCO1}) to attain a band alignment with E_V in the p-layer. Hence, the transport is based on TAT of electrons (eTAT) and holes (hTAT), also enabling SRH recombination in i/p layer. In c), relatively high N_{TCO2} results in low TCO E_C . Thus, a large ΔE_{TCO2} is across the alignment with the valence band (E_V) at c-Si or p-layer, meaning small energy barriers and thus allowing DT of holes and B2BT mechanisms. Condition c) leads to minimal ρ_c which is concurrently independent of defects (SRH recombination).

3 Contact stack evaluation

Each contact stack is typically evaluated by transmission line measurement (TLM) process. Accordingly, it is relevant to evaluate ρ_c for different contact stack properties. In this respect, WP4 measured ρ_c of different combinations of layers featuring a variety of E_a and N_{TCO} developed within the consortium. Subsequently, to understand the dominant physical mechanisms *per case*, experimental data are compared to numerical simulations. Accordingly, a simulation platform based on TCAD Sentaurus was built to consistently include all aforementioned mechanisms for TLM structures and IBC-SHJ solar cells. To individually evaluate the potential of each contact in IBC-SHJ devices, contact stack under analysis is considered as variable while the other is assumed the most performant (minimal ρ_c). Similarly, the base contribution to series resistance is reduced by assuming a relatively small rear half pitch of 300 µm as reported in Section 4 and also 100 µm as base thickness. It is worth noting that all assumptions correspond to optimal and still realistic values of ρ_c and rear patterning.

3.1 n-Contact

Figure 3 a) shows ρ_c as a function of E_a and N_{TCO} for the n-contact. Within the simulation domain of experimentally available values, ρ_c is more sensitive to the E_a of doped layer than N_{TCO} as the transport is based on DT in a potential barrier built on c-Si/i-aSi band offset. In general, a decrease of E_a leads to electron accumulation on c-Si side and energy barrier reduction (Procel et al., 2018). Such a trend is replicated by evaluating the FF of simulated IBC-SHJ, assuming minimum p-contact resistivity (see Figure 3 b). V_{oc} also reproduces the trend of ρ_c albeit for a variation of only 5 mV (see Figure 3 c). Finally, a similar trend is observed for η in the same simulation domain (see Figure 3 d). Hence, n-contact stack using doped layers with E_a < 220 meV or TCO with N_{TCO} > $5x10^{20}$ cm^{-3} facilitates ρ_c < 40 $m\Omega \cdot cm^2$ with potential FF > 85% and also η > 26%. It is worth noting that increasing N_{TCO}, TCO E_F is "pulled up" meaning that WF_{TCO} decreases which is favourable for n-contact.

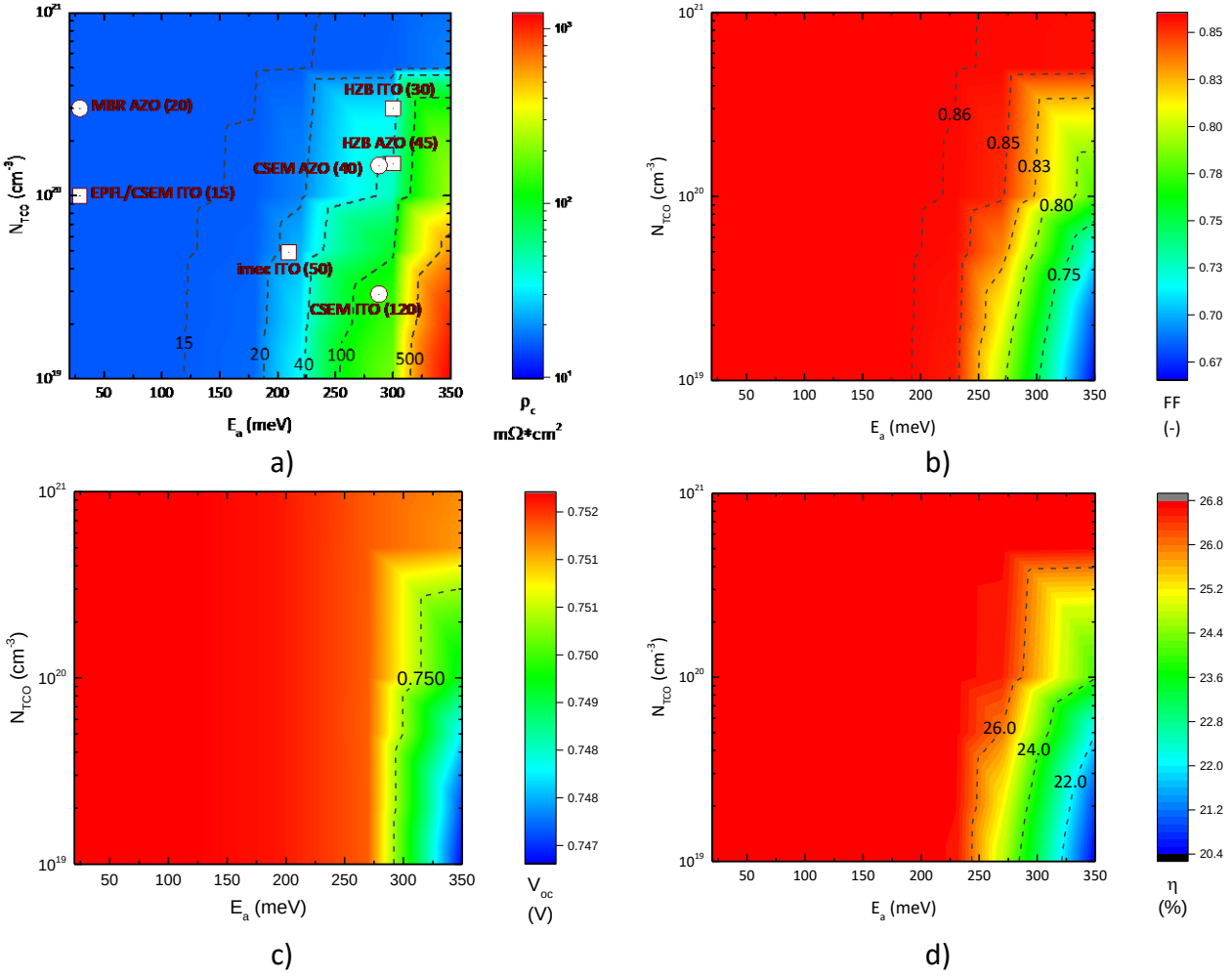

Figure 3. n-contact stack roadmap (assuming minimal ρ_c at p-contact -see Section 3.2- and minimal base lateral transport -see Section 4). a) ρ_c as a function of E_a and N_{TCO}. Points in the chart indicate measured ρ_c values (in brackets) (WP4 input) in reasonable agreement with simulated values. Circles indicate estimated values of E_a. b) FF as a function of E_a and N_{TCO}. FF replicates the inverse of ρ_c trend in the whole simulation domain. c) V_{oc} as a function of E_a and N_{TCO}. V_{oc} replicates FF and ρ_c trend in the complete simulation domain with only 5 mV variation. d) η as a function of E_a and N_{TCO}. η replicates FF and ρ_c trend in the complete simulation domain.

3.2 p-Contact

Figure 4 a) shows that both E_a and N_{TCO} influence ρ_c as the transport is affected by band alignment allowing B2BT and/or TAT (see Figure 2 b). In particular, within experimentally attainable E_a and N_{TCO}, values ρ_c depends more on N_{TCO} for E_a < 250 meV (i.e. for nano-crystalline layers), while for E_a > 250 meV (i.e. for amorphous layers), ρ_c depends more on E_a. Indeed, decreasing E_a improves c-Si band bending concurrently reducing the negative effect of potential barrier and WF mismatch (Procel et al., 2018). In general, ρ_c increases for high values of E_a and low N_{TCO} values where TAT is dominant, thus revealing that B2BT is more efficient than TAT for transport of carriers. Figure 4 b) reports a FF trend similar to ρ_c. There, for E_a > 300 meV, in addition to the transport mechanisms, FF is also constrained by V_{oc} decrease, as observed in Figure 4 c). Indeed, in such a case, c-Si band bending decreases

making traps to support more SRH recombination rather than TAT transport inside deposited doped layer. Then, η is evaluated in Figure 4 d) showing a similar trend to FF and ρ_c. Hence, p-contact stack using doped layers with E_a < 260 meV together with TCO featuring N_{TCO} > 1x10^{20} cm^{-3} facilitates ρ_c < 50 mΩ·cm^2 with potential FF > 85% and η > 26%.

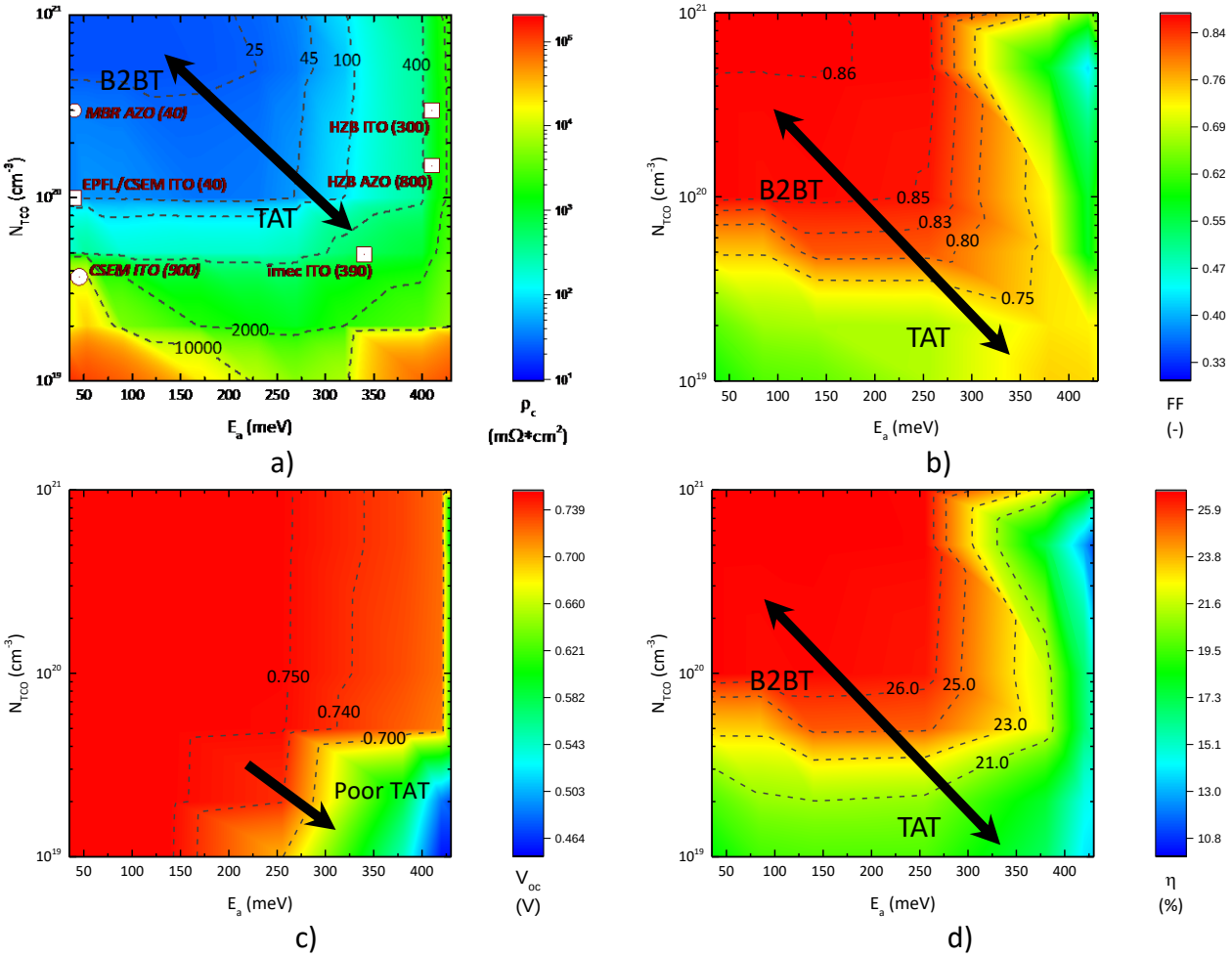

Figure 4. p-contact stack roadmap (assuming minimal ρ_c at n-contact -see Section 3.1- and minimal base lateral transport -see Section 4). a) ρ_c as a function of E_a and N_{TCO}. Points in the chart indicate measured ρ_c values (in brackets) (WP4 input) in reasonable agreement with simulated values. Circles indicate estimated values of E_a. b) FF as a function of E_a and N_{TCO}. FF replicates the inverse of ρ_c trend for E_a < 300 meV. Note that FF behaviour becomes sensitive to V_{oc} for E_a > 300 meV. c) V_{oc} as a function of E_a and N_{TCO}. For E_a > 300 meV, V_{oc} is affected by trap recombination in doped layers as result of poor c-Si band bending (Procel et al., 2018) *and thus poor selectivity. d) η as a function of E_a and N_{TCO}. η replicates FF and ρ_c trend in the complete simulation domain.*

4 Rear side patterning

To evaluate the impact of rear geometry on lateral transport in IBC-SHJ solar cells, we performed simulations changing the n-type finger width, p-type finger width and pitch size and assuming optimized contact stacks as reported in Section 3. For the sake of simplicity, within these simulations, the width of metal and TCO fingers corresponds to the width of doped layer fingers. Figure 5 presents FF as a function of half pitch and coverage of p-type contact over pitch. Minimal pitch leads to higher FF, but optimal p-type finger coverage remains constant to a value of 60%. Such a value results on the comparison of minimal ρ_c between p-contact (22 mΩ·cm^2) and n-contact (11 mΩ·cm^2) as optimal n- and p-contacts from Section 3 for different rear side area. Indeed, this results from the trade-off between holes and electrons transport mechanisms in which n- and p-contact series resistance contribution are equivalent. Figure 5 reports the maximum attainable FF even with optimal n- and p-contact stack. Hence, to achieve FF > 85%, half pitch < 800 µm is mandatory.

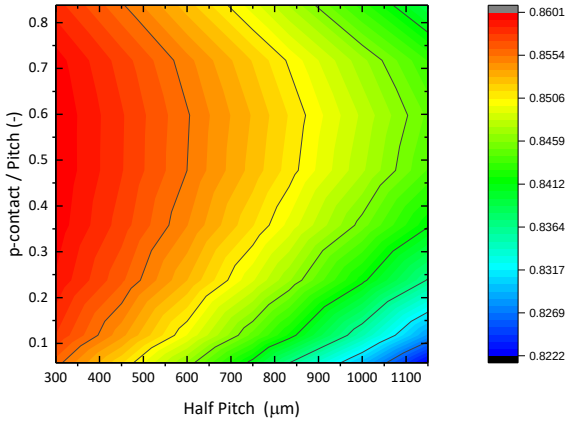

Figure 5. FF as a function of half pitch and coverage of p-contact over pitch. It is observed that longer pitches increase the path of carriers to be collected, thereby affecting the FF. The FF is optimal for coverage of p-contact over pitch of around 60%.

Aiming at half pitch < 800 µm is technologically challenging by using tunnelling IBC technology (Paviet-Salomon et al., 2015; Tomasi et al., 2017) (photo-lithography free process) which is, in contrast, attractive for industry and have demonstrated the best conversion efficiency within the consortium above 25 % (FF ~ 82 %, V_{oc} > 730 mV) for half pitch > 1000 µm. Indeed, the calculated ultimate V_{oc} and FF for such device is 736 mV and 83% respectively, thus revealing that most of the losses are intrinsic to materials properties (mostly on c-Si). However, achieving half pitch < 1000 µm is limited by the alignment of TCO and metallization steps that depend on the shape of the profile of n-layer deposition (n-finger width). Therefore, to relax such limiting factor, some patterning options are available (see Table I) to increase FF in ~ 0.5%. Nevertheless, conversion efficiency hardly could achieve more than 26%. At this point, when patterning is on the technological edge, a step into different wafer resistivity or wafer thickness is crucial to decrease intrinsic losses. In fact, using similar wafer resistivity (4 Ω*cm), but reducing the wafer thickness from 260 to

200 µm, ultimate V_{oc} and FF would increase in 6 mV and 0.5%abs respectively (see Table I), then achieving efficiency > 26% is more feasible. It is worth noting that light management schemes should include double ARC or MST to keep J_{sc} > 41.5 mA/cm^2 (D5.2 and D3.3).

						Bulk thickness 260 µm			**Bulk thickness 200 µm**		
Option	**Pitch (µm)**	**n-finger width (µm)**	**n-metal finger width (µm)**	**p-metal finger width (µm)**	**Gap TCO (µm)**	**Ultimate FF**	**Ultimate V_{oc}**	**η**	**Ultimate FF**	**Ultimate V_{oc}**	**η**
Current Design	2500	**900**	**700**	1600	200	83%	736mV	25.65%	83.50%	742mV	**26.02%**
1	2270	**900**	**720**	1300	250	83.30%	736mV	25.75%	83.85%	742mV	**26.10%**
2	2020	**800**	**640**	1200	180	83.40%	736mV	25.80%	83.90%	742mV	**26.20%**
3	1760	**700**	**560**	1000	200	83.80%	736mV	25.90%	84.30%	742mV	**26.30%**
4	1260	**500**	**400**	600	260	84.10%	736mV	**26%**	84.75%	742mV	**26.40%**

Table I. Proposed patterning design with different bulk thickness considering patterning technological limitations for tunneling IBC (n-finger width). Reducing c-Si bulk thickness from 260 to 200 µm increases potential V_{oc} and FF.

5 Risks and interconnections

5.1 Risks/problems encountered

No risks or problems were encountered for this work.

5.2 Interconnections with other deliverables

This deliverable is related to the following deliverables/milestones/tasks:

- Task 4.1:
  - "Advanced a-Si:H and uc-Si:H based materials and TCO/metal stacks"
- Milestone 5:
  - "Demonstration of an IBC-SHJ device 6-in wafer with the most promising processes for patterning and light trapping"
- Deliverable 5.2:
  - D5.2 "Light management scheme allowing Jsc > 42 mA/cm^2 (interlinked to D4.3)"
- Deliverable 8.1:
  - D8.1 "Report on the breakdown of optical and electrical losses in IBC-SHJ solar cells and optimization strategies"

6 Conclusions

The route for obtaining high efficiency (IBC-) SHJ solar cells is established in terms of layers properties using ρ_c and rear side patterning as transport evaluation. Practical insights are provided on how to improve the transport of collected carriers in terms of E_a and N_{TCO} and their relation in the estimation of ρ_c. Furthermore, as minimal ρ_c values are additionally associated to low recombination in thin silicon films, evaluating ρ_c is a practical indicator for contact stack quality.

In general, ρ_c is minimal (η maximal) using doped layers exhibiting low E_a values which experimentally are achievable with nano-crystalline Si thin film layers. In such condition, the device is resilient against any negative effect of WF mismatch or TCO material choice (e.g. AZO, IOH or ITO). N-contact stack using doped layers with E_a < 220 meV or TCO with N_{TCO} > $5x10^{20}$ cm^{-3} facilitates ρ_c < 40 $m\Omega \cdot cm^2$ with potential FF > 85% and also η > 26%. P-contact stack using doped layers with E_a < 260 meV together with TCO featuring N_{TCO} > $1x10^{20}$ cm^{-3} facilitates ρ_c < 50 $m\Omega \cdot cm^2$ with potential FF > 85% and η > 26%.

Lateral transport inside the bulk is evaluated in terms of pitch and width of n-type and p-type contacts. Small pitch values increase FF. Specifically for IBC-SHJ cells, n-type and p-type contacts should cover the pitch according to ρ_c of n- and p-contact comparison. With minimal contact resistance contribution, half pitch values < 800 µm lead to FF > 85% and η > 26%. Such a patterning is feasible for processes that include costly photo-lithography technology. Nevertheless, industry attractive single patterning using shadow mask (tunneling IBC - half pitch values > 1000 µm) also potentially could achieve efficiency above 26 % with fine tuning of half pitch and reducing bulk thickness to 200 µm.

7 References

Adachi, D., Hernández, J. L., & Yamamoto, K. (2015). Impact of carrier recombination on fill factor for large area heterojunction crystalline silicon solar cell with 25.1% efficiency. *Applied Physics Letters*, *107*(23), 233506. https://doi.org/10.1063/1.4937224

Gehring, A., & Selberherr, S. (2004). Modeling of Tunneling Current and Gate Dielectric Reliability for Nonvolatile Memory Devices. *IEEE Transactions on Device and Materials Reliability*, *4*(3), 306–319. https://doi.org/10.1109/TDMR.2004.836727

J. McCann, M., R. Catchpole, K., J. Weber, K., & W. Blakers, A. (2001). A review of thin-film crystalline silicon for solar cell applications. Part 1: Native substrates. *Solar Energy Materials and Solar Cells*, *68*(2), 135–171. https://doi.org/10.1016/S0927-0248(00)00242-7

Klein, A., Körber, C., Wachau, A., Säuberlich, F., Gassenbauer, Y., Harvey, S. P., … Mason, T. O. (2010). Transparent conducting oxides for photovoltaics: Manipulation of fermi level,work function and energy band alignment. *Materials*, *3*(11), 4892–4914. https://doi.org/10.3390/ma3114892

Lee, T. D., & Ebong, A. U. (2017). A review of thin film solar cell technologies and challenges. *Renewable and Sustainable Energy Reviews*, *70*(September 2015), 1286–1297. https://doi.org/10.1016/j.rser.2016.12.028

Paviet-Salomon, B., Tomasi, A., Lachenal, D., Barraud, L., Descoeudres, A., Christmann, G., … Ballif, C. (2015). Development of photolithography-free, large-area, back-contacted silicon heterojunction solar cells. In *Proceedings of the 7th Workshop on Back Contact Solar Cell and Module Technology*.

Powell, M. J., & Deane, S. C. (1996). Defect-pool model and the hydrogen density of states in hydrogenated amorphous silicon. *Physical Review B*, *53*(15), 10121–10132. https://doi.org/10.1103/PhysRevB.53.10121

Procel, P., Yang, G., Isabella, O., & Zeman, M. (2018). Theoretical evaluation of contact stack for high efficiency IBC-SHJ solar cells. *Solar Energy Materials and Solar Cells*, *186*(June), 66–77. https://doi.org/10.1016/j.solmat.2018.06.021

Tomasi, A., Paviet-Salomon, B., Jeangros, Q., Haschke, J., Christmann, G., Barraud, L., … Ballif, C. (2017). Simple processing of back-contacted silicon heterojunction solar cells using selective-area crystalline growth. *Nature Energy*, *2*, 17062. Retrieved from http://dx.doi.org/10.1038/nenergy.2017.62

Yamamoto, K., Adachi, D., Uzu, H., Ichikawa, M., Terashita, T., Meguro, T., … Hernández, J. L. (2015). High-efficiency heterojunction crystalline Si solar cell and optical splitting structure fabricated by applying thin-film Si technology. *Japanese Journal of Applied Physics*, *54*(8). https://doi.org/10.7567/JJAP.54.08KD15

Yoshikawa, K., Yoshida, W., Irie, T., Kawasaki, H., Konishi, K., Ishibashi, H., … Yamamoto, K. (2017). Exceeding conversion efficiency of 26% by heterojunction interdigitated back contact solar cell with thin film Si technology. *Solar Energy Materials and Solar Cells*, *173*(June), 37–42. https://doi.org/10.1016/j.solmat.2017.06.024